COMPUTATION OF AERODYNAMIC SOUNDS AT LOW MACH NUMBERS USING FINITE DIFFERENCE LATTICE BOLTZMANN METHOD

H. K. Kang[1*], M. Tsutahara[2], K. Shikata[2], E. R. Kim[3], Y. T. Kim[4] and Y. H. Lee[5]

Aerodynamic sounds generated by a uniform flow around a two-dimensional circular cylinder at Re=150 are simulated by applying the finite difference lattice Boltzmann method. Thethird-order-accurate up-wind scheme (UTOPIA) is used for the spatial derivatives, and the second-order-accurate Runge-Kutta scheme is applied for the time marching. We have succeed in capturing very small pressure fluctuations with the same frequency of the Karman vortex street compared with the pressure fluctuation around a circular cylinder. The propagation velocity of the acoustic waves shows that the points of peak pressure are biased upstream due to the Doppler effect in the uniform flow. For the downstream, on the other hand, it is faster. It is also apparent that the amplitude of sound pressure is proportional to $r^{-1/2}$, r being the distance from the center of the circular cylinder. To investigate the effect of the lattice dependence, furthermore, 2D computations of the tone noises radiated by a square cylinder and NACA0012 with a blunt trailing edge at high incidence and low Reynolds number are also investigate.

Keywords: Lattice Boltzmann Method, Compressible Fluid, Aerodynamic Sound

1. INTRODUCTION

With the increase of speed of transport vehicles like airplane, automobiles, and trains in recent years, noise has become a large environmental problem. There are two kinds of noise: vibration noise created by the vibration of object, and aerodynamic noise produced by the unsteady motion of fluid. The energy of sound due to the object vibration is proportional to $O(10^{-2})$ of the representative velocity while the aerodynamic noise is proportional to $O(10^{-5}$-$10^{-8})$. Understanding the aerodynamic noise by analyzing its mechanism is therefore difficult.

In the numerical research of the aerodynamic sound, it can be possible to analyze the information of the detailed flow field, which is not obtained in the experiments, by directly solving the compressible Navier-Stokes equation. However, in studying the aerodynamic sound by the numerical method, a number of things are necessary: a highly accurate scheme to realize the sound pressure ($O(10^{-4})$) against the static pressure; a wide calculation area to obtain far away sound pressure field; and removal of the numerical reflection at the boundary.

The flow around a circular cylinder[1,2] or an airfoil[3] has been studied experimentally and numerically for quite a while because it is one of the abundant phenomena of the fundamental fluid mechanics. Yet, in spite of its simplicity, a lot of unsolved problems still exist. One of them is the generation mechanism of acoustic waves by the flow around the cylinder. This has also been studied experimentally and numerically to some extent. The numerical analyses has been done in the conventional way that a vorticity dominant near field is simulated first and then an acoustic far field is obtained using approximated equations derived

Received: July 21, 2004, Accepted: January 27, 2005.

1 School of Mechanical and Aerospace Engineering Institute of Marine Industry, Gyeongsang National Univ.
2 Graduate School of Science and Technology, Kobe Univ.
3 Department of Civil engineering, Chonbuk National Univ.
4 Department of Marine System Engineering, Korea Maritime Univ.
5 Division of Mechanical & Information Engineering, Korea Maritime Univ.
* Corresponding author. E-mail: kanghokeun@chol.com

from the acoustic analogy.[4] So far most of the computational work on the sound generation due to flow past a circular cylinder has been done using the hybrid method[5], acoustic/viscous splitting methods[6,7] and the direct numerical simulation (DNS)[8,9], but in this field, the studies using lattice boltzmann method (LBM)[10] are very few.

In the present study, using finite difference lattice Boltzmann method (FDLBM) over the entire region from the near to far fields, the generation and propagation mechanism of the acoustic waves produced by a turbulent wake of a circular cylinder in a uniform flow at low Reynolds number is computed. The predicted sound spectra with the vortex/flow dynamics is clarified and the effect of the Mach number using the sound velocity is also examined. In order to see the characteristic of the lattice dependence, besides, 2D computations of the tone noise radiated by a square cylinder and an airfoil (NACA0012) with a blunt trailing edge at high incidence and low Reynolds number are also investigated.

In the following analysis, let L be a characteristic length, U a characteristic flow speed and c a characteristic particle speed which is the order of sound speed.

2. ANALYSIS

There has been rapid development the lattice gas method (LGM or lattice gas cellular automaton LGCA)[11] and the LBM for simulating fluid dynamics problems. In traditional numerical methods, the macroscopic variables (velocity and density) are obtained by solving the Navier-Stokes equations. The LBM solves the microscopic kinetic equation for particle distribution function from which the macroscopic quantities (velocity and density) are obtained through the movement and the collision of particles. Some books and reviews presented a lot of studies in this field.[12-14]

The presently popular method uses regularly spaced lattices and cannot handle curved boundaries with desirable flexibility. To circumvent such difficulties, the FDLBM[15,16] in curvilinear coordinates is explored using body-fitted coordinates with non-uniform grids.[17] It become possible and easy to simulate the complicated object shapes, and the application to various flow fields is attained. This method has high flexibility for coordinate system selection and is often the choice among various different schemes.

2.1 DISCRETIZED LATTICE BGK MODEL

The Boltzmann equation governing the velocity distribution function f_i may be written, with a single relaxation time Φ, as:

$$\frac{\partial f_i}{\partial t} + c_i \cdot \nabla f_i = -\frac{1}{\Phi}(f_i - f_i^{eq}) \tag{1}$$

In this equation, the real number f_i is the normalized number of particles at each lattice node and time t, moving in direction i. The microscopic dynamic associated with Eq.(1) can be viewed as a two-step process of movement and collision. In the collision step, the distribution functions at each site relax toward a state of local equilibrium. The form of RHS term, given in Eq.(1), represents a relaxation of the distribution towards its equilibrium value and recovers the nonlinear form of the fluid, ensuring that the fully nonlinear Navier-Stokes equation is satisfied. The equilibrium distribution functions f_i^{eq} depends on the fluid density ρ, velocity u, and internal energy e, at each site which can be calculated from the distribution functions as:

$$\rho = \sum_i f_i \tag{2}$$

$$\rho u = \sum_i c_i f_i \tag{3}$$

and

$$\rho e = \sum_i \frac{1}{2} c^2 f_i - \frac{1}{2}\rho u^2 \tag{4}$$

Up to $O(u^3)$, we assume that the equilibrium distribution function is expressed as:

$$f_i^{eq} = F_i \rho [1 - 2Bc_{i\alpha}u_\alpha + 2B^2(c_{i\alpha}u_\alpha) + Bu^2 - \frac{4}{3}B^3(c_{i\alpha}u_\alpha) - 2B^2 c_{i\alpha}u_\alpha u^2] \tag{5}$$

where the Greek subscripts represent vector components. The moving particles are allowed to move with five kinds of speed, c, $2c$, $3c$, $\sqrt{2}c$ and $2\sqrt{2}c$, and the particles are 21 kinds, as shown

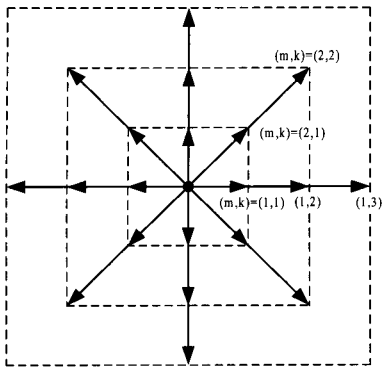

Fig. 1 A compressible lattice Boltzmann model (D2Q21). The m=1 indicates the particle which moves in the orthogonal direction and m=2 indicates the particle which moves in the diagonal direction. The k represents the speed of particle which moves in the nearest neighboring lattice

in Fig. 1. The functions F_i and B, respectively, are determined by:

$$F_1 = 1 + \frac{5}{4Bc^2}\left(\frac{17}{96B^2c^4} + \frac{35}{48Bc^2} + \frac{49}{45}\right) \quad (6)$$

$$F_{2-5} = -\frac{1}{8Bc^2}\left(\frac{13}{16B^2c^4} + \frac{71}{24Bc^2} + 3\right) \quad (7)$$

$$F_{6-9} = \frac{1}{16Bc^2}\left(\frac{5}{16B^2c^4} + \frac{25}{24Bc^2} + \frac{3}{5}\right) \quad (8)$$

$$F_{10-13} = -\frac{1}{24Bc^2}\left(\frac{1}{16B^2c^4} + \frac{1}{8Bc^2} + \frac{1}{15}\right) \quad (9)$$

$$F_{14-17} = \frac{1}{4B^3c^6}\left(\frac{Bc^2}{3} + \frac{1}{8}\right) \quad (10)$$

$$F_{18-21} = -\frac{1}{153B^3c^6}\left(2Bc^2 + 3\right) \quad (11)$$

$$B = -\frac{1}{2e} \quad (12)$$

The models for compressible fluids are sometimes unstable in calculation because the distribution function becomes a negative value. Using the finite difference, it stabilizes the calculation considerably. For this purpose, this paper employs the discretized BGK equation (1). This equation is shown to lead the Navier-Stokes equations by the Chapman-Enskog expansion, and the term $(\Phi - 1/2)$ in transfer coefficient changes into Φ. The relationship between the kinematic viscosity and relaxation time factor becomes:

$$\nu = \frac{2}{D}\rho e \Phi \quad (13)$$

In this equation, D is the characteristic dimension and the value of D is 2 for two-dimensional case. For high Reynolds number flows which are very important in engineering fields, $\nu << 1$ must be satisfied. If Euler's first order forward difference scheme is used for time integral, the equation is transformed as:

$$f_i^{n+1} = f_i^1 + \Delta t\left[-c_{i\alpha}\frac{\partial f_i^n}{\partial x_\alpha} - \frac{1}{\Phi}(f_i^n - f_i^{eq})\right] \quad (14)$$

where Δt is the time increment. In Eq. (14), the condition of stability for the collision term must be satisfied $\Delta t/\Phi < 2.0$, which states that the distribution function approaches its equilibrium state by every collision. Relations between ν and $\Delta t/\Phi$ lead that, for high Reynolds number flows, the time increment chosen must be very small and the calculation time will be very long. Therefore, an equation in which the third term is added to the discretized BGK equation (Eq. (1)) is transformed:

$$\frac{\partial f_i}{\partial t} + c_{i\alpha}\frac{\partial f_i}{\partial x_\alpha} - Ac_{i\alpha}\frac{\partial}{\partial x_\alpha}\left(\frac{f_i - f_i^{eq}}{\Phi}\right) = -\Phi(f_i - f_i^{eq}) \quad (15)$$

in which $A(>0)$ is a constant. Then the relationship is changed as follows.

$$\nu = \frac{2}{D}\rho e(\Phi - A) \quad (16)$$

By conducting such conversion, it is possible to modify the relationship between the coefficient of the kinematic viscosity and the single relaxation coefficient $\Phi - \nu$ to $\Phi \to A - \nu$ in FDLBM. Therefore, the single relaxation coefficient Φ becomes $\Phi \to A$ in the flow of high Reynolds number, and the transformed model of FDLBM makes it possible to calculate with the fixed value of Φ which is taken in high Reynolds number flows. Furthermore, it becomes possible that the calculation of Δt can easily or stably simulate up to large value, while $\Delta t/\Phi = 2.0$ is an upper limit for the collision term in the conventional FDLBM model.

The macroscopic equations can be derived from the lattice Boltzmann equations by conducting a Chapman-Enskog expansion in the time and space derivatives such that

$$\frac{\partial}{\partial t} \rightarrow \varepsilon \frac{\partial}{\partial t_1} + \varepsilon^2 \frac{\partial}{\partial t_2} \tag{17}$$

$$\frac{\partial}{\partial x_\alpha} \rightarrow \varepsilon \frac{\partial}{\partial x_{1\alpha}} \tag{18}$$

and the distribution function is expanded in powers of ε as

$$f_i = f_i^{eq} + \varepsilon f_i^{(1)} + \varepsilon^2 f_i^{(2)} + \cdots \tag{19}$$

where the dimensionless number ε is of the same order as the Knudsen number. Substituting the expression for the equilibrium distribution functions of Eq. (5), and the Chapman-Enskog expansions of Eqs. (17), (18) and (19), the Navier-Stokes equations are obtained as

$$\frac{\partial \rho}{\partial t} + \frac{\partial \rho u_\alpha}{\partial x_{1\alpha}} = 0 \tag{20}$$

$$\frac{\partial \rho u_\alpha}{\partial t} + \frac{\partial \rho u_\alpha u_\beta}{\partial x_\beta} = -\frac{\partial p}{\partial x_\alpha} + \frac{\partial}{\partial x_\beta}\left(\frac{\partial u_\alpha}{\partial x_\beta} + \frac{\partial u_\beta}{\partial x_\alpha}\right) + \frac{\partial}{\partial x_\alpha}\lambda\left(\frac{\partial u_\beta}{\partial x_\beta}\right) \tag{21}$$

$$\frac{\partial}{\partial t}\rho\left(\frac{1}{2}u^2 + e\right) + \frac{\partial p}{\partial x_\alpha}\left(\frac{1}{2}u^2 + e + \frac{p}{\rho}\right)\rho u_\alpha = \frac{\partial}{\partial x_\alpha}\left(k^* \frac{\partial e}{\partial x_\alpha}\right) + \frac{\partial}{\partial x_\alpha}\left[\nu u_\beta\left(\frac{\partial u_\alpha}{\partial x_\beta} + \frac{\partial u_\beta}{\partial x_\alpha}\right)\right] + \frac{\partial}{\partial x_\alpha}\left(\lambda u_\alpha \frac{\partial u_\beta}{\partial x_\beta}\right) \tag{22}$$

Here the details are skipped, but, from the above equations, the pressure, the second viscosity, the conductivity of internal energy and the speed of sound can be wirrten in non-dimensional forms by using characteristic quantities L, c and ρ:

$$p = \frac{2}{D}\rho e \tag{23}$$

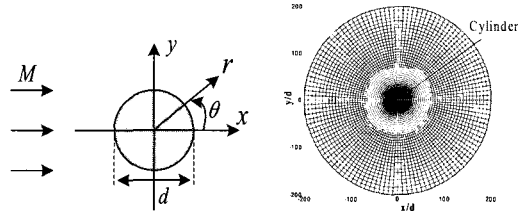

(a) (b)

Fig. 2 Schematic diagram of the flow field model (a) and computational mesh for flow past a circular cylinder (b). For clarity, only one in every four mesh lines for the radial direction is plotted.

$$\lambda = -\frac{4}{D^2}(\Phi - A) \tag{24}$$

$$k^* = \frac{2(D+2)}{D^2}\rho e(\Phi - A), \tag{25}$$

$$c_s = \sqrt{\frac{2(D+2)}{D^2}e} \tag{26}$$

3. NUMERICAL METHOD

In this section, we consider a schematic diagram of the flow around a circular cylinder in a 2D uniform flow (Fig. 2(a)) using the finite difference lattice Boltzmann model in Eq.(15) described in section 2. In the Cartesian coordinate (x,y), the uniform flow of the velocity U_0 parallel to the x direction is considered. Normalized by the static sound velocity c_0, the streamwise velocity is prescribed by the $M = U/c_0 = U/\sqrt{2e}$, where M is the Mach number. Furthermore, the cylinder of the diameter L is fixed at the origin. The polar coordinates (r,θ) are also used, where the azimuthal angle θ is defined from downstream in the counterclockwise direction. The Reynolds number, defined as $RE = UL/\nu$, where ν is the kinematic viscosity, is equal to 150.

For the entire field from near to far acoustic field, computations are carried out on a O-grid configuration shown in Fig. 2(b), where only one-quarter of the mesh lines for the radial direction are plotted for clarity. A typical grid system in the case of Re=150 is constructed as follows: the number of the grid points results in $r \times \theta = 201$ (in the radial direction) $\times 121$ (in the azimuthal direction); the time increment Δt is 0.02; and the examined Mach numbers use the sound velocity by changing

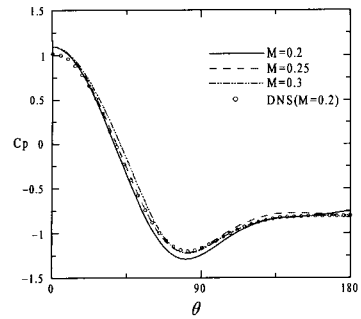

Fig. 3 Time average pressure c_p at M=0.2, 0.25, 0.3 and DNS result(Inoue, 2002) at $0 \le \theta \le \pi$, Re=150.

the internal energy *e*. All the calculations are in two-dimension and use 2D21V model. Computations start with uniform velocity $u_i(t=0)=(U,0)$ everywhere.

For spatial derivatives, a third-order-accurate up-wind scheme (second-order-accurate at the boundary) is used, and a second-order-accurate Runge-Kutta scheme is used fortime integration. Adiabatic and no-slip conditions are adopted on the cylinder surface. Along the O-grid shaped outer boundary, the velocities are set at the freestream values, $u_i=(U,0)$. Because the boundary is sufficiently far away from the circular cylinder, the numerical wave reflections from the boundary are removed.[18,19] The spacing in the surface region is prescribed to be fine enough to analyze the boundary layer on the cylinder surface. The acquired data is set forth sufficiently after the effect of the initial perturbation become negligible $(t \ge 100)$.

4. NUMERICAL SIMULATIONS

4.1 FLOW-INDUCED NOISE

A flow past a circular cylinder at Re=150 is considered for validation of the modified FDLBM model (Eq. (15)), in which the cylindrical coordinated system is employed. The numerical results when the Karman vortex street was fully developed are shown in Figs. 3 to 8. Force acting on the cylinder surface as a function of the azimuthal angle θ is presented in Fig. 3 for three different Mach numbers (M=0.2, 0.25 and 0.3), and compared with that of DNS result[9]. Pressure coefficient C_p is the time averaged pressure on

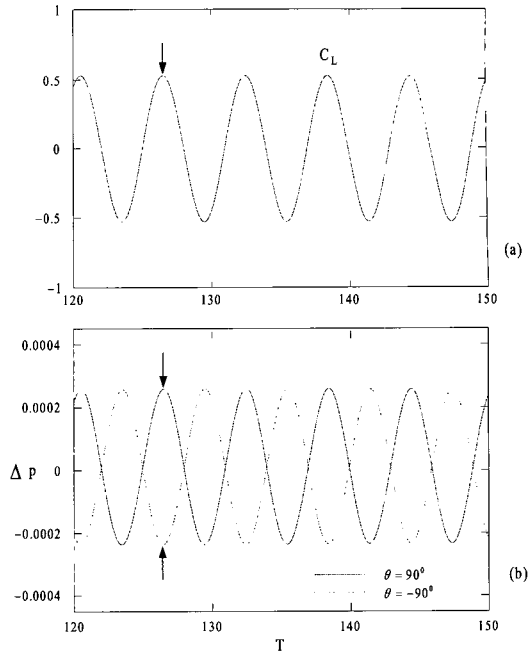

Fig. 4 Lift force acting on the cylinder surface (a) and time history of the sound pressure (b). M=0.2, Re=150. Arrows indicate T=127. L=50; solid line $\theta = 90°$; blue line $\theta = -90°$.

the cylinder surface normalized by the value at the stagnation point $\theta = 0^0$, and defined as:

$$C_p = \frac{p - p_0}{1/2\rho_0 U^2} \tag{27}$$

in which p_0 denotes the ambient pressure. From the figure, it shows that the coefficient c_p is not affected significantly by the Mach number. A comparison of the pressure coefficient at $0 \le \theta \le \pi$ for M=0.2 also indicates that FDLBM is compatible with DNS.

In the near-field flow structure, lift force C_L acting on the cylinder surface and pressure variations are plotted in Fig. 4 for the case of M=0.2(e_0=0.5). Here, the non-dimensional pressure fluctuation Δp is defined as:

$$\Delta p = (p - p_0)/p_0 \tag{28}$$

Time history of sound pressure at the point d=50 and $\theta = \pm 90°$ is shown in Fig. 4(b). By comparing with the lift coefficient C_L in Fig. 4(a), during the period T(=Ut/L)=120~150, it can be seen that the

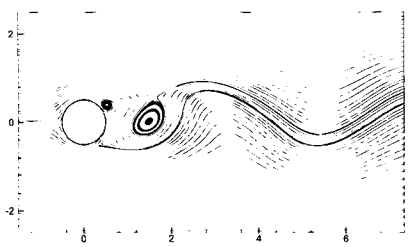

Fig. 5 Instantaneous streamlines in the vicinity of a circular cylinder at T=132.

period of c_L oscillates equal to the period of Δp. And positive peaks of C_L also coincide with the positive and negative peaks of $\Delta p_{\theta=\pm 90^\circ}$. In this case, the Strouhal number is defined by S_t=fL/U where f is the frequency of the periodic vortex shedding. It is evaluated as $S_t = 0.177$, which is very close to the experimental value (0.18 in Williamson)[1] and DNS result (0.183 in Inoue & Hatakeyama)[9] for Re=150. Figs. 5 and 6 show the streamlines at $T(=Ut/L)=132$ and vorticity field. In Fig. 6, a vortex is shed from the upper side of the circular cylinder during the period (T=127 and 132) and, behind the cylinder, vortices become weaker with increasing downstream distance.

Figure 7 shows the acoustic pressure field at T=132 for three different Mach numbers (M=0.2, 0.25, and 0.3), where the contour level fluctuates at, $\Delta p_{step} = 3\times10^{-4}, 7.5\times10^{-3}$ and 1.0×10^{-3}, respectively. The solid lines indicate the positive pressures and the dashed lines are the negative ones. As can be seen from this figure, rarefaction waves with negative Δp and compression waves with positive Δp are generated alternately around the cylinder at the origin, and propagate downstream and upstream,

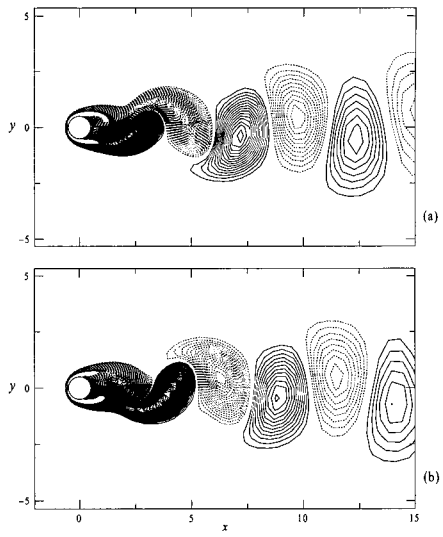

Fig. 6 Vorticity contours at two different instants at M=0.2, Re=150. (a) T=127, (b) T=132.

respectively.

Figure 8 illustrates distributions and decays of the sound pressure plotted along the three different angles ($\theta = 45^\circ, 90^\circ$ and 135°) for the case of Re=150 and 0.2. The distributions of Δp are plotted against the radial distance r from the origin at the three different times T=130, 131, and 132. Each peak of the waves is found to propagate and decay. The propagation speed of the waves is equal to the speed of sound in the far field, in agreement with the linear acoustic theory. Also, the decaying curves are converged to the lines proportional to $r^{-1/2}$ in the far field, which is again in accordance with the theory. These results suggest that the sounds generated from the cylinder at low Reynolds numbers are precisely captured by FDLBM if both

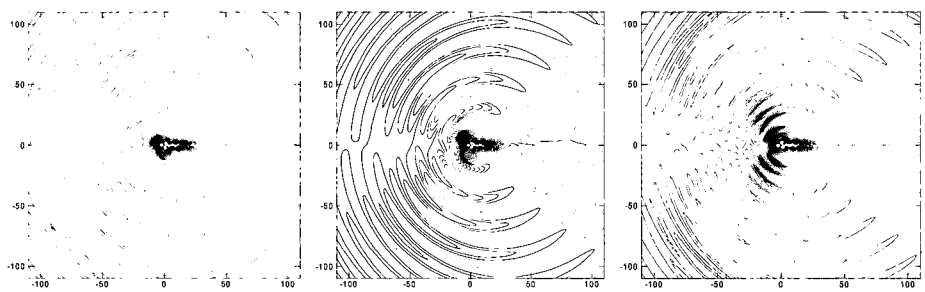

(a) M=0.2 (b) M=0.25 (c) M=0.3

Fig. 7 Contours of sound pressure at T=132 and Re=150 for three different Mach numbers. The contour level fluctuates at $\Delta p_{step} = 3\times10^{-4}, 7.5\times10^{-3}$ and 1.0×10^{-3}, respectively. Solid lines: positive, dotted lines: negative.

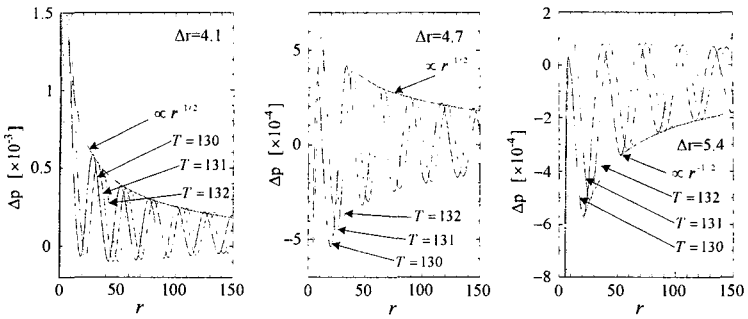

(a) θ=45^0 (b) θ=90^0 (c) θ=135^0

Fig. 8 Distribution and decays of sound pressure at three different directions. M=0.2. Re=150.

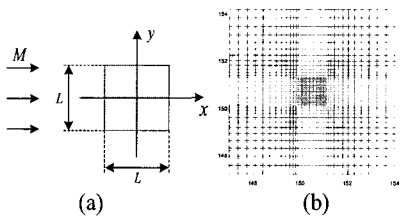

(a) (b)

Fig. 9 Schematic diagram of the flow field (a) and computational mesh (enlarged) (b) for square cylinder (Case 1).

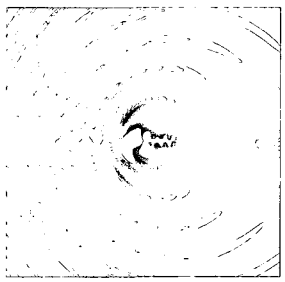

Fig. 10 Sound pressure distribution around square cylinder for M=0.3 and Re=200 at T=142.

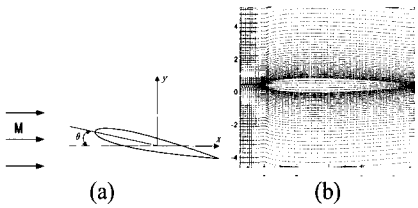

(a) (b)

Fig. 11 Schematic diagram of the flow field (a) and computational mesh with NACA0012 (enlarged) (b) (Case 2).

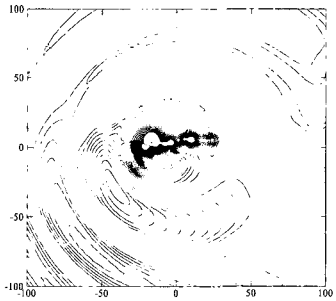

Fig. 12 Contours of sound pressure past a NACA0012 airfoil at 14 deg angle of attack. T=156, Re=200 and M=0.2.

the flow dynamics in the near field and the wave propagations in the far field are computed with high accuracy.

4.2 DEPENDENCE FOR LATTICE IN NOISE

Furthermore, to validate the lattice dependence, we consider the unsteady flowfield and the sound generated by a square cylinder (see Fig. 9 (Case 1)) and a NACA0012 airfoil (see Fig. 11 (Case 2))placed in a two-dimensional uniform flow. Case 1 has Re=200, U=0.2 and M=0.3(e_0 =0.22). Case 2 has Re=200, U=0.2 and M=0.2(e_0 =0.5) and an angle of attack is given α =14 deg. All calculation conditions are the same in case of the circular cylinder.

The simulated flowfields for two cases are presented in Figs. 10 and 12, respectively. The solid lines indicate the positive pressures and the dashed lines are negative ones. As can be seen from Figs. 11 and 12, rarefaction waves with negative Δp and compression waves with positive Δp are generated alternately around the square cylinder (see Fig. 10) and NACA0012 airfoil (see Fig. 12) at the origin, and it propagate downstream and upstream, respectively. With these results presented here, it is considered that the acoustic waves have

an isotropic characteristic regardless of the lattice shapes.

5. CONCLUSIONS

In this paper we have simulate the acoustic waves generated from the flow around a circular cylinder using the FDLBM of the two-dimensional 21velocity model. The sound frequency is the same as the vortex shedding frequency of the Karman vortex street. The rarefaction waves and the compression waves are alternately generated and propagate toward downstream and upstream, respectively. The sound pressure also decays proportional to $r^{-1/2}$ in the far acoustic field, which agrees with the theoretical prediction.

The analysis with the square cylinder and NACA0012 also elucidated that the acoustic waves have an isotropic characteristic regardless of the lattice shapes.

REFERENCES

[1] Williamson, C.H.K., 1996, "Vortex Dynamics in the Cylinder Wake," *Annu. Rev. of Fluid Mech.*, Vol.28, pp.477-539.

[2] Persillon, H. and Braza, M., 1998, "Physical Analysis of the Transition to Turbulence in the Wake of a Circular Cylinder by Three-dimensional Navier-Stokes Simulation," *J. Fluid Mech.*, Vol.365, pp.23-88.

[3] Wang, M., Lele, S.K. and Moin, P., 1996, "Computation of Quadrupole Noise Using Acoustic Analogy," *AIAA J.*, Vol.34, No.11, pp.2247-2254.

[4] Curle, N., 1955, "The Influence of Solid Boundaries upon Aerodynamic Sound," *Proc. R. Soc. Lond.*, A231, pp.505-514.

[5] Hardin, J.C. and Lamkin, S.L., 1984, "Aeroacoustic Computation of Cylinder Wake Flow," *AIAA J.*, Vol.22, pp.51-57.

[6] Shen, W.Z. and Sorensen, J.N., 1999, "Comment on the Aeroacoustic Formulation of Hardin and Pope," *AIAA J.*, Vol.37, pp.141-143.

[7] Slimon, S.A., Soteriou, M.C. and Davis, D.W., 1999, "Computational Aeroacoustics Simulations Using the Expansion about Incompressible Flow Approach," *AIAA J.*, Vol.37, pp.409-416.

[8] Colonius, T., Lele, S.K. and Moin, P., 1997, "Sound Generation in a Mixing Layer," *J. Fluid Mech.*, Vol.330, pp.375-409.

[9] Inoue, O. and Hatakeyama, N., 2002, "Sound Generation by a Two-dimensional Circular Cylinder in a Uniform Flow," *J. Fluid Mech.*, Vol.471, pp.285-314.

[10] Tsutahara, M., Kurita, M. and Kataoka, T., 2003, "Direct Simulation of Acoustic Waves by the Finite Difference Lattice Boltzmann Method," *Trans. JSME J., B*, Vol.69-680, pp.841-847.

[11] Chopard, B. and Droz, M., 1998, *Cellular Automata Modeling of Physical Systems*, Cambridge University Press.

[12] Alexander, F.J., Chen, S. and Sterling, D.J., 1993, "Lattice Boltzmann Thermodynamics," *Phys. Rev.,E*, Vol.47, pp.2249-2252.

[13] Chen, Y. and Doolen, G.D., 1998, "Lattice Boltzmann Method for Fluid Flows," *Annu. Rev. Fluid Mech.*, Vol.30, pp.329-364.

[14] Tsutahara, M. and Kang, H.K., 2002, "A Discrete Effect of the Thermal Lattice BGK Model," *J. Stat. Phys.*, Vol.107, No.112, pp.479-498.

[15] Cao, N., Chen, S., Jin, S. and Martinez, D., 1997, "Physical Symmetry and Lattice Symmetry in the Lattice Boltzmann Method," *Phys. Rev., E*, Vol.55, pp.R21-R24.

[16] Kang, H.K., Tsutahara, M., Ro, K.D. and Lee, Y.H., 2002, "Numerical Simulation of Shock Wave Propagation Using the Finite Difference Lattice Boltzmann Method," *KSME Intl. J.*, Vol.16, No.10, pp.1327-1335.

[17] Mei, R. and Shyy, W., 1998, "On the Finite Difference-based Lattice Boltzmann Method in Curvilinear Coordinates," *J. Comput. Phys.*, Vol.143, pp.426-448.

[18] Pointsot, T. and Lele, S.K., 1992, "Boundary Conditions for Direct Simulation of Compressible Viscous Flows," *J. Comput. Phys.*, 101, pp.104-129.

[19] Kim, J.W. and Lee, D.J., 2000, "Generalized Characteristic Boundary Conditions for Computational Aeroacoustics," *AIAA J.*, Vol.38, pp.2040-2049.